Critical size for phase separation in binary alloys: Role of elastic interactions and mechanical constraints

Justin C. W. Song[1] and Rajeev Ahluwalia[1,2,*]

[1]*Institute of Materials Research and Engineering, A*STAR (Agency for Science, Technology and Research), 3 Research Link, Singapore 117602*

[2]*Materials Theory and Simulation Laboratory, Institute of High Performance Computing, A*STAR (Agency for Science Technology and Research), Science Park II, Singapore 117528*

(Received 25 April 2008; revised manuscript received 13 June 2008; published 13 August 2008)

We study the effect of mechanical boundary conditions on the phase separation of elastically coupled binary alloys. Two distinct boundary conditions are considered; clamped boundaries in which there is no macroscopic shape change and traction free boundaries where a net shape change of the grains is possible. In particular, we are interested in system size effects and its relation to the boundary conditions. For clamped boundary conditions, we find that there exists a critical size below which no phase separation is possible. It is found that the miscibility gap depends on the system size for such cases. On the other hand, for traction free boundary conditions, no critical size is observed and the miscibility gap is independent of the system size. We also observe contrasting processes in the kinetics of phase separation for the two different boundary conditions. The stark contrast in behavior serves to underscore the sensitive dependence of elastic interactions on boundary conditions and geometry. These findings are relevant for polycrystalline alloys with nanosized grains where the clamped case serves as a simple model for a single grain, embedded deep in a polycrystal, constrained by its surrounding grains.

DOI: 10.1103/PhysRevB.78.064204 PACS number(s): 61.66.Dk, 64.75.Nx, 81.30.Mh

I. INTRODUCTION

Phase transitions in binary alloys can be dramatically influenced by elastic interactions.[1–7] Cahn[1] showed that elasticity can shift the miscibility gap by a constant temperature, Onuki[3] performed computer simulations of domain patterns influenced by elasticity and Orlikowski[5] showed particular morphologies that were adopted because of selection criteria based on shear moduli and average alloy composition. For example, the patterns formed by spinodal decomposition in a cubic system favor either the {111} or the {100} planes when inequalities involving the elastic moduli are satisfied.[2] The elastic interaction is long ranged and hence is sensitive to shape and composition distribution[8,9] and boundary conditions. Its interplay with the short-range diffusion of composition is primarily responsible for the phenomena described above.

However, the above studies consider systems in the bulk where periodic boundary conditions may be used. Simulations that use periodic boundary conditions are not suitable to describe nanoscale systems since surface effects are neglected. There is much current interest in phase transformations in materials with nanosized grains. For example in binary alloys the competition between surface and bulk energies can give rise to a critical size below which no phase separation occurs. These surface-tension effects have been studied to some degree by Christensen[10] and Shirinyan.[11] However, in addition to surface tension, elastic coupling together with mechanical constraints can have an effect on critical size. Each grain in a polycrystalline alloy is also mechanically constrained by the surrounding grains and hence the grains cannot be stress free. In this instance, periodic boundary conditions are no longer apt to describe their behavior since mechanical boundary conditions need to specified at the boundary. The effect of mechanical constraints on phase transformations has been studied in the context of ferroelastics by Jacobs;[12,13] it was predicted that the transformation temperature and the order parameter, for a clamped system, is suppressed from the bulk value as the grain size decreases. Our aim in this paper is to investigate if a similar effect exists for diffusive phase transitions, such as phase separation in binary alloys.

Unlike the ferroelastic case,[12,13] where the mechanical constraints directly influence the order parameter (strain), mechanical constraints in the case of binary alloys indirectly influence the phase transformation through the coupling between the elastic strains and the composition order parameter. Thus it is interesting to study how the indirect coupling together with the mechanical constraints influence the size effects in the phase separation of binary alloys. It is also important to study how the kinetics changes with the mechanical boundary conditions.

In this paper, we report on two-dimensional simulations carried out with two nonperiodic boundary conditions: boundaries that are traction free; displacements clamped at the boundaries. In Sec. II, we describe our model along with the relevant boundary conditions. In Sec. III, the role of boundary conditions on domain patterns as well as size effects are discussed for clamped as well as the traction free conditions. Here, we also discuss the kinetics of the phase separation. Section IV ends the paper with a summary and discussion of the results.

II. MODEL

We use the Ginzburg-Landau theory to study the phase separation of binary alloys,[1–6] with an order parameter, ϕ, which represents the local composition. This is a lowest-

order expansion of the free energy that respects symmetry and describes the phase separating behavior.

The free energy in the constrained elastic system can be modeled as[3,4]

$$F = \int d\mathbf{r}\left[f(\phi) + \frac{k_\phi}{2}(\nabla\phi)^2 + f_{\mathrm{el}}\right], \tag{1}$$

where $f(\phi)$ is the Ginzburg-Landau free energy for the order parameter ϕ. The order parameter represents the difference between local concentrations of the two constituent components in the alloy. The second term, $\frac{k_\phi}{2}(\nabla\phi)^2$, is a gradient energy attributed to surface tension[1,14] and f_{el} is the elastic energy of the system which is composition dependent. $f(\phi)$ can be written in the usual form

$$f(\phi) = \frac{a_0}{2}\frac{T - T_c}{T_c}\phi^2 + \frac{1}{4}a_4\phi^4, \tag{2}$$

where $\frac{T-T_c}{T_c} = \tau$ is the scaled temperature and a_0 and a_4 are positive phenomenological constants. The choice of these depends on the material. We write the elastic energy for the cubic system, f_{el}, in the form

$$f_{\mathrm{el}} = \frac{C_{11}}{2}[(\epsilon_{xx} - \alpha\phi)^2 + (\epsilon_{yy} - \alpha\phi)^2] + C_{12}(\epsilon_{xx} - \alpha\phi)(\epsilon_{yy} - \alpha\phi) + C_{44}\epsilon_{xy}^2. \tag{3}$$

Here we introduce coupling between the strains, ϵ, and the order parameter, ϕ, by allowing the effective strains to be altered by the order parameter accounting for lattice mismatch between the two components. For a stress free system, positive ϕ results in extension and negative ϕ results in compression in order to minimize energy. α describes the coupling strength and parameterizes the lattice mismatch. We note that the elastic coupling is expressed in a slightly different form from Refs. 4 and 6, though from a symmetry point of view they are identical. In fact, a similar form has been used in the literature.[7,15] The advantage of this form for the elastic coupling is it does not renormalize the transition temperature for a stress free system.

The kinetics of the phase-separation process can be described by coupled equations for the order parameter and the displacements. The evolution of the order parameter can be described by the Cahn-Hilliard equation[1]

$$\frac{\partial\phi}{\partial t} = \mu\nabla^2\frac{\delta F}{\delta\phi}, \tag{4}$$

where μ is the mobility. This conserves the order parameter, ϕ, and typifies the diffusive interaction and propagation of the composition through space. The evolution of the displacements can be described as

$$\rho\frac{\partial^2 u_i}{\partial t^2} = \sum_j \frac{\partial\sigma_{ij}}{\partial r_j} + \eta\nabla^2 v_i, \tag{5}$$

$$\sigma_{ij} = \frac{\delta F}{\delta\epsilon_{ij}}, \tag{6}$$

where ρ is the density, σ_{ij} is the stress tensor and $\mathbf{v}$ is the velocity. η describes the viscosity of the viscous damping term. This equation describes the condition of force balance, also incorporating for the viscous damping in the solid. We remark that unlike previous approaches which assume mechanical equilibrium to hold everywhere, at all times, in our approach, the above equation describes the kinetics of the displacements. The advantage of this method is that it is natural to do calculations in real space and hence nonperiodic boundary conditions are easier to implement.

We perform simulations of the above model using a simple central difference in space and an euler difference in time to approximate the differentials. Since we are only interested in qualitative results we choose simple values for the parameters: $a_0=1$, $a_4=1$, $k_\phi=2$, $C_{11}=2$, $C_{12}=1$, $C_{44}=4$, $\eta=10$, and $\mu=1$. The phase separating behavior is strongly dependent on the coupling constant, α, so we choose a representative value of the coupling constant $\alpha=0.7$. The simulations were conducted on a two-dimensional square lattice. The step sizes in the finite differences were $\delta x=\delta y=1$ and $\delta t=0.01$. We investigated two types of mechanical boundary conditions. Surface boundary conditions on the order parameter were common to both types of boundary conditions. This surface boundary condition on the order parameter was

$$n_i\nabla_i\phi\Big|_s = 0; \quad n_i\nabla_i\frac{\delta F}{\delta\phi}\Big|_s = 0, \tag{7}$$

where n_i is the in-plane vector normal to the surface at the boundaries and s is the boundary of the system. These stipulate that there is no surface energy from the order parameter gradients at the boundary and no current entering or leaving the surface. This allows us to isolate the mechanical effects in the system.

First we implemented traction free boundary conditions where in addition to the order parameter and current dependent boundary conditions in Eq. (7), we stipulate that the tractions at the boundaries go to zero. This can be expressed as

$$\sigma_{ij}n_j = 0. \tag{8}$$

Vanishing stresses at the boundary allow and induce the system to change its geometry when minimizing the free energy.

Second we used a boundary condition where the displacements were clamped [in addition to Eq. (7)]. The clamped boundary conditions are

$$u_i\Big|_s = 0; \quad v_i\Big|_s = 0. \tag{9}$$

These clamp the displacements and consequently the velocities. Here, the system is fixed in place and displacements are only allowed within the surface. This means that the total volume in the systems remains constant in contrast to the traction free boundary conditions. The clamped boundary conditions also fix the shape of the system.

III. SIMULATIONS OF DOMAIN PATTERNS

We numerically integrate Eqs. (4) and (5) without thermal noise with the boundary conditions detailed above. We initialized the system with a random noise about zero in displacements and order parameter, ϕ. Each simulation was evolved till equilibration where the maximum order parameter in the system had saturated and the velocities had vanished to zero.

A. Traction free boundary conditions

For the case of traction free boundary conditions, we observe phase separation for all sizes simulated. The phase separated states for $\tau=-1$ are depicted in Fig. 1. We observe that with these boundary conditions, the system decomposes to just two domains of opposite order parameter. However, the order parameter within each domain is not homogeneous, and there exist fluctuations due to inhomogeneous distributions of the strain which arise due to geometrical constraints imposed by the shape of the system. The domain pattern does not change with size and an almost perfectly phase separated state with just one domain wall is observed for all sizes. The cubic symmetries imposed by the elastic moduli chosen are almost respected and a {100} plane is selected because $2C_{44}-C_{11}+C_{12}>0$ (Ref. 2) for the parameters used. Using the configurations shown in Fig. 1 as the initial conditions at $\tau=-1$, we simulate the dynamical equations at different temperatures to test the stability of the phase separated states. A miscibility curve obtained by calculating the maximum and the minimum values of the order parameter at different temperatures is shown in Fig. 2. The curves do not show a significant shift with size and take on a shape similar to the one expected for the homogeneous case. We expect this because of the vanishing stresses at the boundaries which allow the system and domains therein to move and change to give the lowest energy configuration and decompose fully.

An interesting observation we make from both Fig. 1 and 2 is that the maximum absolute order parameter at $\tau=-1$ is greater than one. Since there is no current out of and into the system and total number of particles of both components in the alloy should stay the same. Thus a value of $|\phi|>1$ appears to violate the order-parameter conservation. To understand this apparent inconsistency, we analyze the definition of the order parameter $\phi=(n_a-n_b)/(n_a+n_b)$. In an undistorted lattice, the quantity $n_a+n_b=N_{\mathrm{av}}$, where N_{av} is the total number of atoms in a coarse-grained element. This is the same for each element in the homogenous lattice. In most implementations, as in ours, the definition of the order parameter becomes $\phi=(n_a-n_b)/N_{\mathrm{av}}$ where N_{av} is fixed for each element by stipulating a constant overall order parameter and a constant grid size, $\delta x \delta y$. In a distorted lattice, however, local volume changes allow for $n_a+n_b\neq N_{\mathrm{av}}$. In particular, n_a+n_b may be more than N_{av} in a given local region of the space which can result in $|\phi|>1$. Due to the overall conservation of the order parameter, this results in an inhomogeneous distribution in the order parameter that can be clearly seen in Fig. 1. This is solely due to the distorting strains allowed for by the traction free boundary conditions that induce local volume changes. We note that this also means that the initial square shape of the system is no longer preserved and a different shape is chosen which helps minimize energy. This allows the system additional degrees of freedom, not afforded by the boundary conditions described below, that permit this clear two-phase domain pattern in Fig. 1. We repeated these simulations with different values of α and the compositional inhomogeneities decrease at lower values of α. At $\alpha=0$, perfectly homogeneous phase separation is observed.

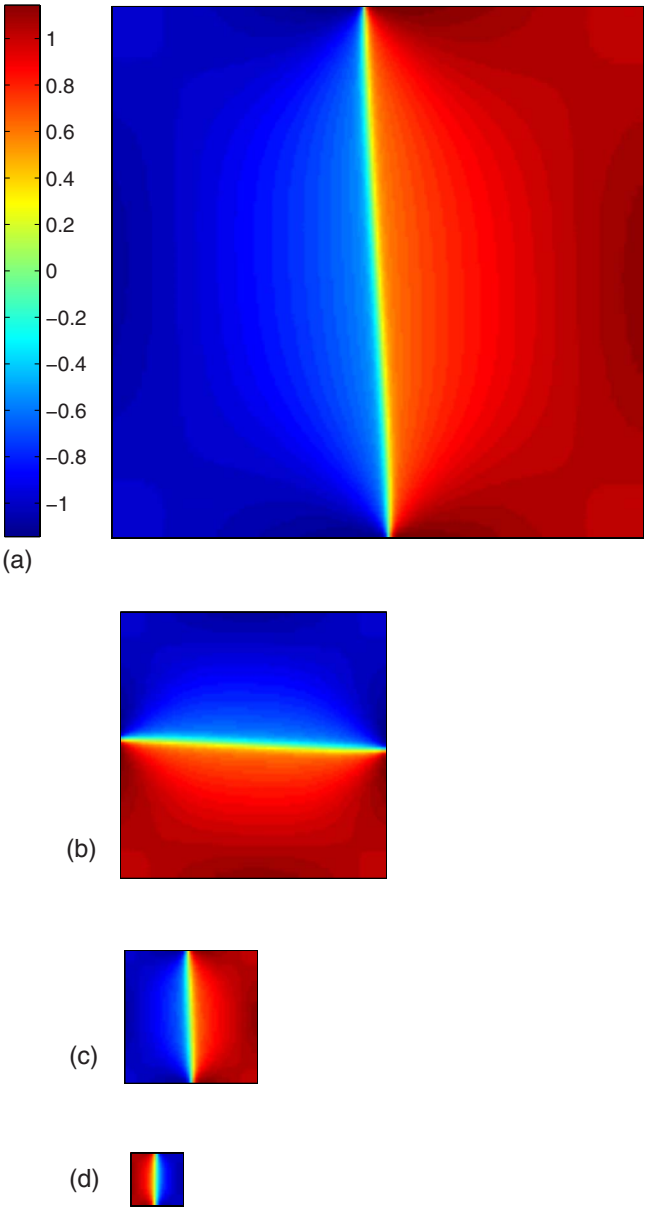

FIG. 1. (Color online) Plots of spinodal decomposed binary alloys at $\tau=-1$ for varying sizes using traction free boundary conditions. The panels are (a) 200×200 lattice, (b) 100×100 lattice, (c) 50×50 lattice, and (d) 20×20 lattice. We note that there are compositional fluctuations within the same domain. The 200×200 lattice was simulated to 1.5×10^5 units in time. The rest were simulated to 1.0×10^5 units in time.

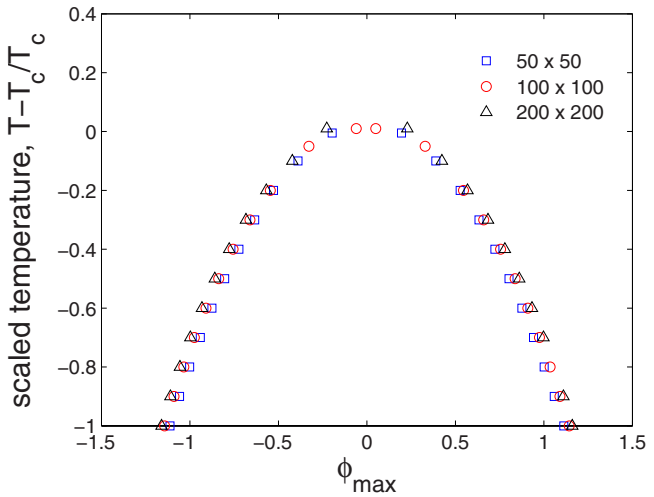

FIG. 2. (Color online) Miscibility gap for traction free boundary conditions with varying system sizes denoted by △ 200×200 (black), ○ 100×100 (red), and □ 50×50 (blue). This is plotted using the maximum and minimum order-parameter values in the whole system.

B. Clamped boundary conditions

We obtained the domain patterns as well as the miscibility curves for the clamped case, using the same procedure as above. Figure 3 shows the converged patterns for different sizes. Notice the significant changes in the domain patterns where the number of two phase domains decrease with size from the largest size (200×200) to the smallest size (20×20) where no decomposition occurs. Thus there exists a critical size below which no phase separation occurs. For the present set of parameters, this critical size was determined to be 35×35. This is in stark contrast to the phase separation that is allowed even for a 20×20 system for the traction free boundary conditions. This difference clearly points to the change in mechanical boundary conditions, namely the clamping, as the culprit for this size effect. Obviously, this critical size is nonuniversal and depends on the coupling constant, α, and elastic moduli chosen. However, other constants such as the viscosity, density, and mobility are not expected to change this as they only contribute to the kinetics.

The choice of elastic moduli constrains the domains to form in the {100} planes and this is respected here as well. The boundaries between saturated compositions are not very pronounced and we find that the profiles are in fact sinusoidal along a given direction in the system.

We note that near the boundaries, we observe curved domain walls. This was also observed in the context of ferroelastics.[12,13,16] We believe that this is happening due to the shear strains that arise due to the clamping effects at the boundary. Therefore, the domain walls can deviate from the usual {100} planes.

A remarkable result in the clamped systems is the decreased value of the local composition within the phase separated domains. We can observe from Fig. 3 that the local composition appears to decrease with the system size until below the critical size, no phase separation occurs. To further

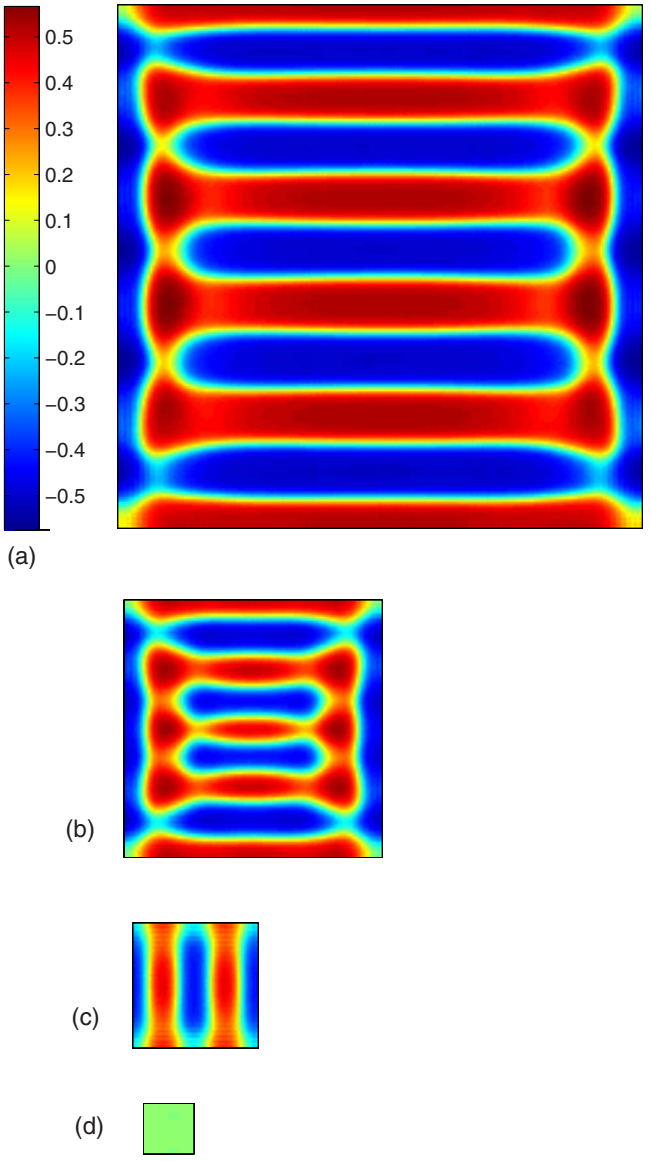

FIG. 3. (Color online) Plots of spinodal decomposed binary alloys at $\tau=-1$ for varying sizes using clamped boundary conditions. The panels are (a) 200×200 lattice, (b) 100×100 lattice, (c) 50×50 lattice, and (d) 20×20 lattice. The number of allowed domains decreases with size until there is no phase separation at the 20×20 lattice. All plots were simulated to 1.0×10^5 units in time.

clarify this behavior, we obtained the miscibility curves for this case at different sizes using the same procedure that was used to calculate the miscibility curves for the traction free case. The miscibility curves at three different sizes are shown in Fig. 4. The miscibility gap in Fig. 4 exhibits a size dependent shift in the critical temperature. The saturated compositions also decrease with size. One can see that for lower sizes the miscibility gap shrinks toward the abscissa. Eventually, this shrinks till it is level with the abscissa and no phase separation is observed as for the 20×20 lattice in Fig. 3. Here, Fig. 4, we show a cross over from the two-phase to the single phase. We plot the maximum "saturated" phases in the time simulated. We find that the transition to the one-phase region is not sharp and instead there is a cross over behavior.

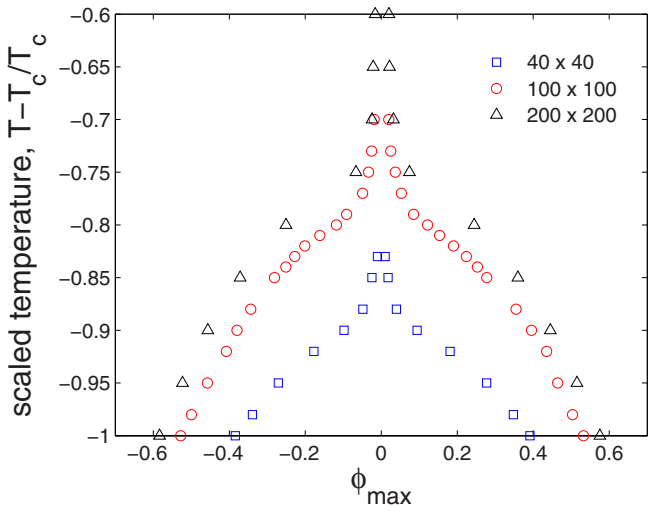

FIG. 4. (Color online) Miscibility gap for clamped boundary conditions with varying system sizes denoted by △ 200×200 (black), ○ 100×100 (red), and □ 40×40 (blue).

We believe that this is due to the metastability of the two-phase state that is induced by the elastic interactions and the clamping.

We now discuss the physical mechanism of the size effect we observe. A well-known explanation for the existence of critical sizes in-phase transitions is the competition between the surface and the bulk energies. These account for the effects seen in Ref. 10. However, in the present paper, by virtue of boundary conditions in Eq. (7), the surface energy of the free or clamped surface is not taken into account. For the traction free case, no critical size was observed due to the fact that there was no surface energy associated with the system nor were there clamped boundaries. This suggests that the size effect is a result of the mechanical clamping and the elastic interactions. In particular, it is a competition between the gradient energy and the elastic energy and clamping. Unlike the traction free case, phase separation with only two domains cannot be observed since such a domain pattern cannot maintain the clamped boundary conditions. Clamping forces the introduction of additional domain walls compared to the traction free case to accommodate the constant shape and size of the system. This results in additional gradient energy which is mitigated by the lowering of saturated composition in each domain. Thus we see that the clamping results in an incomplete phase separation within the phase separated region. This also explains the difference between the saturated compositions of the traction free and the clamped cases, for say 100×100 system from comparing Figs. 2 and 4.

As we decrease the size of the clamped system we find that the characteristic domain size decreases as well. The smaller the domain size, the greater the gradient energy density. In fact, we expect the gradient energy density cost to go as $\sim 1/r$, where r is the characteristic size of the domains within a given system. As a result of the smaller domain sizes, the saturated compositions decrease so as to lower the gradient energy of the composition. Together with smaller domain sizes for smaller systems, this results in the size dependence of the miscibility gaps of Fig. 4. Hence, we find that the degree of phase separation decreases with size. Beyond a certain critical size, in our case a 35×35 system, the energy cost of creating such small domains becomes so high that phase separation does not occur at all. Thus we have a critical size purely from mechanical constraints. We expect this effect to become more pronounced as we increase the coupling constant. It should be noted that this effect occurs indirectly through a clamping of the displacements. The compositions at the boundaries are not prespecified and evolve only according to energy minimization.

The shift in the critical temperature we observe and Cahn's constant shift,[1] although both due to elastic interactions, are qualitatively different. We observe a size dependence in the temperature shift. This size effect is unexpected from just a simple consideration of the change in the coefficient of ϕ^2 term in the total free energy when we add in the elastic energy. The size dependence that we have observed is a result of the explicit clamping of the displacements at the boundaries.

It should be noted that as we increase the size we expect that the clamping at the surface becomes less important. We believe that as the system size becomes very large, we expect it not to feel the clamping effect far from the boundaries and the system should behave very much like a bulk stress free system. We already observe in Fig. 4 the miscibility gap shifting out with increasing size. This should approach the theoretical miscibility curve for a homogeneous system as $L\rightarrow\infty$.

We repeated these simulations for different values of the coupling constant, α. The phase separation is suppressed for all nonzero values of α, although for very small values of α the change in the miscibility curve with size is less pronounced. For $\alpha=0$ the miscibility curve is the same as that one would expect from the analytic solution for homogeneous case. This is due to the decoupling of the elasticity from the composition at $\alpha=0$.

C. Kinetics

In Secs. I and II we showed the converged domain patterns. However, it is also of interest to examine and compare the kinetics for the different boundary conditions. There are qualitative differences in the kinetics for the two boundary conditions. Apart from the different final phase separated states, the time taken to reach this state is an order of magnitude longer for the traction free boundary conditions as compared to the clamped boundary conditions. This is due to the fact that the traction free case is dominated by long-range diffusion since the phase separated domains are coarsening. For the clamped case, the diffusion is short range. The clamped case selects a characteristic domain size very quickly, after which the kinetics is governed by the motion of interfaces between different orientations of the lamellar domains. Figures 5 and 6 show that the route to the final phase separated states with the two different boundary condition is different where contrasting processes play a role in the dynamics.

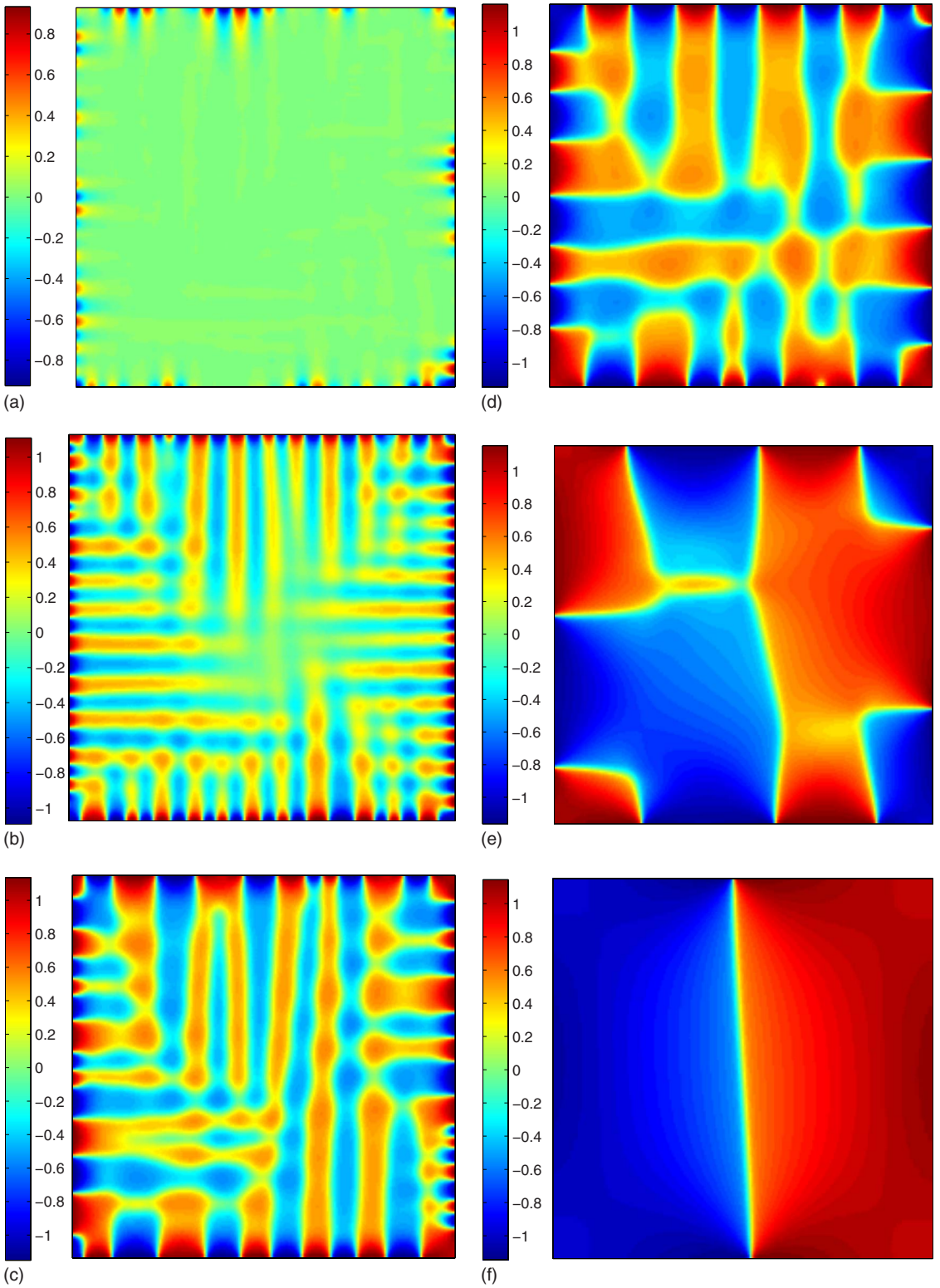

FIG. 5. (Color online) Evolution of spinodal decomposition of a 200×200 lattice with traction free boundary conditions. The panels are (a) 4×10^2, (b) 1×10^3, (c) 3×10^3, (d) 6×10^3, (e) 3×10^4, and (f) 1.5×10^5 units in time.

First we note that, at small times for the traction free boundary condition (Fig. 5), phase separation initiates at the boundaries. This is in sharp contrast to the phase separation which occurs homogeneously at small times for the clamped boundary conditions (Fig. 6). It is clear that this results from the differences in the mechanical boundary conditions. We also see, in agreement with the previous discussion, that in the clamped case once a domain is formed it does not

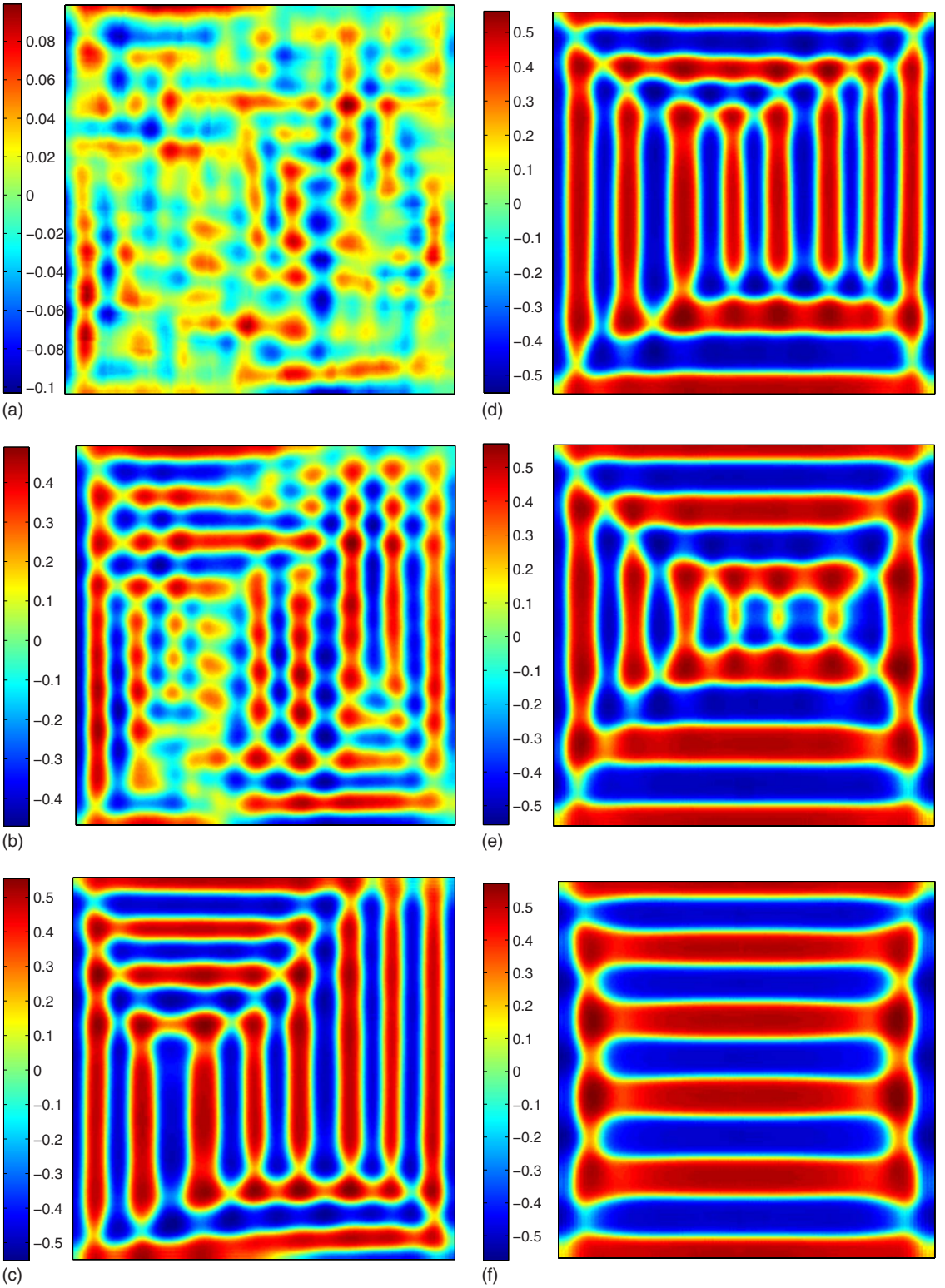

FIG. 6. (Color online) Evolution of spinodal decomposition of a 200×200 lattice with clamped boundary conditions. The panels are (a) 2×10^2, (b) 6×10^2, (c) 2×10^3, (d) 6×10^3, (e) 1.2×10^4, and (f) 2×10^4 units in time.

coarsen significantly in contrast to the traction free case where the domains coarsen to achieve complete phase separation.

In Fig. 5, after initial phase separation at the boundaries, the phase separated domains work their way inwards to form larger domains. The domain boundaries become more distinct. We note that the cubic symmetries are respected during the growth. After this, the domains start to merge to form larger domains to get to the two domain phase separated state we see in the last panel of Fig. 5. This part of the process

takes the longest time because the movement of domain boundaries occurs through a slow long-range diffusion process.

In Fig. 6, after decomposing with small fluctuations everywhere in the system, the fluctuations get amplified[1,2] and take on domain-wall orientations imposed by cubic symmetries in the system. As discussed earlier, the system very quickly selects a characteristic domain size and thereafter the kinetics is governed by the motion of interfaces between different lamellar orientations. Eventually it prefers to have just one set of planes allowed by the symmetries as this configuration minimizes the free energy subject to the boundary conditions. We note that this is the slowest part of the process. However, this is soon arrested, and the microstructure settles to a configuration (that may be metastable) much earlier than the long-time limit pattern of two domains that the traction free case adopts.

IV. CONCLUSIONS

We have studied phase separation in binary alloys with elastic interactions, focusing on the role of mechanical boundary conditions and size effects. Unlike previous approaches which use explicit long-range interactions in terms of the order parameter, we use an approach where kinetics of the displacements is evolved in time along with the order parameter. This is the natural framework for which real-space boundary conditions such as the traction free and clamped are to be implemented. We simulated phase separation at different system sizes for both the traction free as well as the clamped boundary conditions. We show that while for the traction free case, the phase separation can occur even at very small sizes, for the clamped case, a critical size exists below which no phase separation is observed. Since by the virtue of boundary conditions, the surface energy has been ignored in the present work, the critical size exists purely due to the constraints imposed by the mechanical clamping. We have also studied the kinetics of phase separation for the traction free as well as the clamped boundary conditions and find that the kinetics is slower in the former. We believe that these results have relevance for polycrystalline binary alloys with grain sizes of the order of a few nanometers. Of course, real grains in a polycrystal are somewhat intermediate between the two boundary conditions discussed in the present paper, nevertheless the grains will be constrained and cannot be completely stress free. Thus we believe that a critical size for phase separation due to mechanical constraints can indeed exist in binary alloys with nanosized grains where elastic interactions are important.

ACKNOWLEDGMENT

J.S. acknowledges IHPC for computer time.

*rajeev@ihpc.a-star.edu.sg

[1] J. W. Cahn, Acta Metall. **9**, 795 (1961).
[2] J. W. Cahn, Acta Metall. **10**, 179 (1962).
[3] H. Nishimori and A. Onuki, Phys. Rev. B **42**, 980 (1990).
[4] C. Sagui and R. C. Desai, Phys. Rev. E **49**, 2225 (1994).
[5] D. Orlikowski, C. Sagui, A. Somoza, and C. Roland, Phys. Rev. B **59**, 8646 (1999).
[6] A. Onuki and A. Furukawa, Phys. Rev. Lett. **86**, 452 (2001).
[7] P. Fratzl, O. Penrose, and J. L. Lebowitz, J. Stat. Phys. **95**, 1429 (1999).
[8] A. J. Ardell, R. B. Nicholson, and J. D. Eshelby, Acta Metall. **14**, 1295 (1966).
[9] A. Maheshwari and A. J. Ardell, Phys. Rev. Lett. **70**, 2305 (1993).
[10] A. Christensen *et al.*, J. Phys.: Condens. Matter **7**, 1047 (1995).
[11] A. S. Shirinyan and M. Waulet, Nanotechnology **15**, 1720 (2004).
[12] A. E. Jacobs, Phys. Rev. B **52**, 6327 (1995).
[13] A. E. Jacobs, Phys. Rev. B **61**, 6587 (2000).
[14] M. Hilbert, Acta Metall. **9**, 525 (1961).
[15] D. J. Seol, S. Y. Hu, Y. L. Li, J. Shen, K. H. Oh, and L. Q. Chen, Acta Mater. **51**, 5173 (2003).
[16] M. Bouville and R. Ahluwalia, Acta Mater. **56**, 3558 (2008).